Nanocarved Vanadium Nitride Nanowires Encapsulated in Lamellar Graphene Layers as Supercapacitor Electrodes

Dan Zhao (dan.zhao@sust.edu.cn)
Shaanxi University of Science and Technology https://orcid.org/0000-0003-2877-3104
Xiaoyan Yuan
Shaanxi University of Science and Technology
Ruiqin Wang
Shaanxi University of Science and Technology
Qian Zhao
Shaanxi University of Science and Technology
Shouwu Guo
Shanghai Jiao Tong University

Research Article

Keywords: Vanadium nitride, Graphene, Supercapacitor, Nanowire

Posted Date: March 29th, 2021

DOI: https://doi.org/10.21203/rs.3.rs-331550/v1

Version of Record: A version of this preprint was published at Journal of Materials Science: Materials in Electronics on July 28th, 2021. See the published version at https://doi.org/10.1007/s10854-021-06619-6.

Abstract

Supercapacitors have the characteristics of high specific capacitance, long cycle life and fast charging ability, which have shown extremely valuable applications in energy storage fields. Improving the electrode materials is a crucial approach to achieve high capacity. Vanadium nitride (VN) has higher theoretical capacitance than noble metal oxides, as well as better chemical stability and good electrical conductivity. Herein, a composite of VN nanowires with multiple cavities encapsulated in N-doped reduced graphene oxide lamellar layers (VNNWs@rGO) has been synthesized by facile freeze-casting and subsequent nitridation technique. The hierarchical VNNWs@rGO composite exhibited excellent supercapacitor performance: high capacitances of 222 and 65 F g^{-1} were achieved at current densities of 0.5 and 10 A g^{-1}, respectively. The improved electrochemical performance is associated with the unique structural design: the N-doped rGO sheets endowed enhanced electric conductivity and chemical stability for VN, the interconnected laminar network of VNNWs@rGO are crucial for electrolyte penetration and charge transfer, and the cavities and nanoparticles inside the VN nanowires can provide abundant active sites for electric double layer capacitor and pseudocapacitance.

1. Introduction

Developing efficient electrochemical energy storage materials and devices is crucial to developing renewable new energy system. As a type of electric energy storage device, the characteristic of a supercapacitor is between the secondary battery and traditional dielectric capacitor[1–4]. It not only has a power density comparable to that of the electrostatic capacitor, but also has a large energy density, which has a considerable application prospect in the field of energy storage. Electrode materials are one of the critical components of a supercapacitor[5, 6]. Compared with carbon electrode materials, transition metal nitrides have higher mass capacity and vibrational density, and exhibit greater volume energy density[7, 8]. Compared with transition metal oxides, transition metal nitride exhibit higher electrical conductivity, excellent corrosion resistance, hardness and mechanical strength, and remarkable temperature stability[9, 10]. Among various transition metal nitrides, vanadium nitride (VN) is cost-effective and has relatively high conductivity (~ 1.67×106/Ω·m), showing an extremely high specific capacitance[11–18]. In aqueous electrolyte, the energy storage mechanism of VN based electrodes combine the characteristics of double-layer capacitor and pseudocapacitance[19–22]. However, the application of transition metal nitrides in electrochemical energy storage field still has the following problem: although exhibit high capacity, transition metal nitrides is a typical ceramic material with nonnegligible brittleness, which inhibited its structural stability during long-term cycling process of a supercapacitor device[23].

Herein, a supercapacitor electrode of a lamellar composite of nanocarved VN nanowires encapsulated in N-doped reduced graphene oxide layers (VNNWs@rGO) was synthesized by freeze-casting followed by NH_3 nitridation techniques[24]. The as-prepared products possessed foam structure composed of lamellar shaped VNNWs@rGO sheets, which exhibited excellent specific capacitance. Thanks to the synergistic effect between rGO and VN hierarchical structure design, the rGO can not only improve the electric conductivity of the hybrid, but also protect the VN from crumbling into the electrolyte. As a result,

high capacitances of 222 and 65 F g^{-1} at current densities of 0.5 and 10 A g^{-1} have been obtained by VNNWs@rGO that prepared with 2 M GO suspension (which is further donated as VNNWs@rGO-2). Possible underlying mechanisms for the promising electrochemical performance were also discussed.

2. Experimental

2.1 Preparation of materials

The V_2O_5 NWs were synthesized according to previously published procedures, using H_2O_2 and commercial V_2O_5 powders as precursor materials[25]. Firstly, 0.728 g of V_2O_5 powders were dispersed in 60 mL of DI water, followed by adding H_2O_2 (10 mL) under magnetic stirring for two hours. Afterwards, the mixture was transferred into a 100 mL Teflon-lined autoclave for further hydrothermal-treated at 200°C for 96 h. The V_2O_5 nanowires were obtained by washing for several times with flowing EtOH and DI water, following by freeze-drying. The average length and diameter of V_2O_5 nanowires are several micrometers and 150 nm, respectively. Detailed characterization of the as-prepared V_2O_5 nanowires is given in our previously published work.

VNNWs@rGO-2 was prepared by freeze-casting and subsequent nitridation technique. First, graphene oxide (GO) sheets were dispersed into DI water by ultra-sonication for four hours to obtain a GO suspension with a concentration of 2 M. Second, 0.1 g of V_2O_5 NWs were homogenously dispersed into 80 mL of 2 M GO suspension by magnetic stirring for 24 hours. Third, the slurry mixture was transferred to a disk and freeze-dried for 48 h, yielding a lamellar structure with V_2O_5 nanowires encapsulated in GO sheets (VONW@GO). Finally, VONW@GO was transferred to the middle of a horizontal tube furnace and subjected to a nitridation treatment under NH_3 flow at 600°C for 2 hours with a heating rate of 2°C min^{-1}, yielding a lamellar structure of an nanocarved VN nanowires network supported by N-doped rGO sheets (VNNWs@rGO-2). The preparation method of VNNWs@rGO-4 resembles that of VNNWs@rGO-2, except that the concentration of GO suspension was adjusted to 4 M.

2.2 Characterization

Raman spectra of both VNNWs@rGO-2 and VNNWs@rGO-4 samples were obtained by a Renishaw inVia equipment (England). The morphology of both VNNWs@rGO-2 and VNNWs@rGO-4 samples were identified by field emission scanning electron microscopy (FESEM, Hitachi S4800 as well as SU8100, Japan) and transmission electron microscopy (TEM, FEI Tecnai G2 F20 S-TWIN, USA). X-ray diffraction (XRD) patterns of both VNNWs@rGO-2 and VNNWs@rGO-4 samples were obtained by a Bruker equipment.

2.3 Electrochemical measurements

The galvanostatic discharge/charge (GCD), cyclicvoltammetry (CV), and electrochemical impedance spectroscopy (EIS) figure of both VNNWs@rGO-2 and VNNWs@rGO-4 samples were obtained by

electrochemical work station (CHI660E, CH Instrument). A three-electrode architecture, including a VNNWs@rGO working electrode, a Pt sheet counter electrode and a Hg/HgO electrode as reference electrode, was utilized to investigate the electrochemical properties of VNNWs@rGO. The electrolyte is composed of 1.0 M potassium hydroxide. An amplitude of 5 mV and a frequency range of 0.01 ~ 100 kHz were adopted.

3. Results And Discussion

3.1 Morphology and structure

The preparation method of VNNWs@rGO hierarchical structure is shown in Fig. 1. The freeze-drying process is crucially important for the ice films can effectively separate the GO layers that encapsulated with V_2O_5 nanowires (VONW@GO). After completely frozen, the ice films were quickly sublimated by vacuum pump, leaving the GO layers with good dispersion. Finally, nanocarved VN nanowires were transformed from intact V_2O_5 nanowires, and VNNWs@rGO sheets were obtained from VONW@GO by heat treatment under NH_3 flow at a certain rate.

VNNWs@rGO sample that prepared with 2 M and 4 M GO suspension are donated as VNNWs@rGO-2, and VNNWs@rGO-4, respectively. The morphology of as-prepared VNNWs@rGO-2 hybrids is shown in Fig. 2. Porous VN nanowires with were interconnected (Fig. 2a), yielding a large specific surface area of 69.8 $m^2 g^{-1}$, as shown in our previous work[24]. As shown in Fig. 2b-c, VN nanowires with segregated VN nanoparticles inside were fabricated by NH_3 nitridation from VO nanowires, showing a nanocarved structure. The HAADF image and corresponding line scan profile of the cross-section of a single VN nanowire with rGO wrinkles is show in Fig. 2d, further comfirming the nanocarved structure of VN nanowire. The VN nanowires with an average diameter of ~ 150 nm and an average length of several micrometers in length were encapsulated in rGO sheets to form a lamellae structure, as show in Fig. 2e-f. In this unique structure, the 2D rGO sheets can not only support the interconnected VN nanowire network, but also prevent the aggregation of VN nanowires.

Raman spectra of VNNWs@rGO-2 VNNWs@rGO-4 is show in Fig. 3a. In both spectra, typical peaks of VO_x oxides can be observed, indicating the presence of oxides on VN surface, even if VO_x are not detected in our XRD measurements (Fig. 3b). This is a common phenomenon for metal nitrides. The Raman bands located around 1353 and 1596 cm^{-1} are corresponding to D and G peaks of graphite-based materials, respectively. The I_D/I_G ratio are 1.18 and 1.0 for VNNWs@rGO-2 and VNNWs@rGO-4, respectively, indicating that VNNWs@rGO-2 contains more sp3 defects within the sp2 carbon than VNNWs@rGO-4. This is possibly due to higher exposion level of GO during N doping in the ammonia thermal process in VNNWs@rGO-2 sample. The measured XRD pattern of VNNWs@rGO-2 and VNNWs@rGO-4 is shown in Fig. 3b, where the diffraction peaks at 37.6°, 43.8°, 63.7°, 76.4°, and 80.5° (marked by ♦) can be indexed as the lattice planes of VN nanowires (PDF No. 73–0528, black vertical lines at the bottom), indicating

the successfully conversion of V_2O_5 to VN by nitridation. The weak peaks located at 24° (marked by♦) are associated with the (002) planes of graphited carbon.

3.2 The electrochemical property of VNNWs@rGO electrodes

The CV curves of VNNWs@rGO-2 and VNNWs@rGO-4 electrodes at different scan rates (10, 20, 50, 100, and 150 mV s^{-1} are shown in Fig. 4a and Fig. 4b, respectively. The hillock appearance of these curves indicated VNNWs@rGO possessed pseudocapacitance character. The integral areas of the CV curves increased with the increasing scan rates, indicating the excellent rate capability of both VNNWs@rGO electrodes. Obviously, the integral area of the CV curve of VNNWs@rGO-2 is bigger than that of VNNWs@rGO-4. The GCD curves of VNNWs@rGO-2 and VNNWs@rGO-4 electrodes at various current densities within a potential window of -0.9 to 0.1 V are shown in Fig. 4c and Fig. 4d, respectively. With the increase of current density, the charging/discharging time decreased. According to the GCD curves, the specific capacitance (C_m) was calculated based on the equation of $C_m = I\Delta t/m\Delta V$, where I is discharge current, Δt is discharge time, m is the mass of active electrode, and ΔV is the discharge potential range. As shown in Fig. 4e, C_m for VNNWs@rGO-2 are 222, 188.8, 144.9 and 143 F g^{-1} at current densities of 0.5, 1, 3, 5 A g^{-1}, respectively, showing improved capacitance than VNNWs@rGO-4 electrodes, which delivered 176, 145.8, 123.3 and 115 F g^{-1} at current densities of 0.5, 1, 3, 5 A g^{-1}, respectively. Moreover, both VNNWs@rGO-2 and VNNWs@rGO-4 electrodes delivered excellent rate capacity as their C_m values acquired at high current density only decreased modestly compared with that acquired at low current densities. The Nyquist plots for VNNWs@rGO-2 and VNNWs@rGO-4 electrodes are shown in Fig. 4f. The fitted charge transfer resistance of the VNNWs@rGO-2 (1 Ω) is lower than that of VNNWs@rGO-4 (2 Ω). Meanwhile, the higher slope of the low-frequency range for VNNWs@rGO-2 in its EIS curve than that for VNNWs@rGO-4 also indicates better capacitance. The cycle life of VNNWs@rGO-2 and VNNWs@rGO-4 electrodes were appraised a current density of 10 A g^{-1}, as shown in Fig. 4g. The initial discharge capacitance of VNNWs@rGO-2 and VNNWs@rGO-4 electrodes are 65 and 64 F g^{-1}, respectively. The capacitance retention rate of VNNWs@rGO-2 electrode (> 92% after 380 cycles) is obvious higher than that of VNNWs@rGO-4 electrode (62% after 100 cycles), indicating that appropriate rGO loading can improve the ion transfer rate. However, excess amount of rGO inevitably makes the laminar layer thicker. As a result, the improved electrochemical performance of VNNWs@rGO-2 over VNNWs@rGO-4 is mainly due to the increased amounts of VN nanowires. As shown in Table 1, the electrochemical performance of VNNWs@rGO-2 is competitive compared with some graphene/VN based composites, including VN nanoparticles growing on graphene surface[26], carbon fiber@VN nanoparticles[27, 28], 3D VN nanoribbon/graphene composite[29], and nano-VN incorporated on carbon nanospheres[30], VN on porous carbon networks derived polymer[31], porous nanocrystalline VN[32], and VN with surface oxide[12].

The excellent electrochemical properties of VNNWs@rGO-2 electrodes are associated with the following reasons, (1) the robust 2D N-doped rGO sheets endowed enhanced structural-stability and electric conductivity and for the composite. (2) The interconnected laminar structure of VNNWs@rGO is beneficial for electrolyte penetration and rapid ion transportation. (3) the holes and nanoparticles inside the VN nanowires provide abundant active sites for EDLC and pseudocapacitance[33]. (4) The nitrogen doing in rGO participated in the redox reactions at alkaline condition, thus assisting pseudocapacitance for VNNWs@rGO-2 electrode[34]. As a result, the stable structure, and abundant electrochemical active sites make VNNWs@rGO-2 a promising supercapacitor electrode candidate.

Table 1
Comparison of the electrochemical performance of VN/carbon-based electrode materials.

Materials	Electrolyte	Potential window	Specific capacitance	Reference	Materials
VNNP@GO	2 M KOH	(-1.2–0) V	109.7 F g^{-1} at 1.0 A g^{-1}	[26]	VNNP@GO
CF@VN	2 M KOH,	(-1.1–0.1) V	104.05 F g^{-1} at 0.5 A g^{-1}	[28]	CF@VN
3D VNPN/G	1 M KOH	(-1.0–0) V	150 F g^{-1} at 0.5 A g_{-1}	[29]	3D VNPN/G
PCNS@VNNP	2 M KOH	(-1.2–0) V	165 F g^{-1} at 1 A g^{-1}	[30]	PCNS@VNNP
VN/C	2 M KOH	(-1.2–0) V	195.7 F g^{-1} at 1 A g^{-1}	[31]	VN/C
VN@sVO2	1 M KOH	(-1.2–0) V	149.5 F g^{-1} at 1 A g^{-1}	[12]	VN@sVO2
VNNWs@rGO-2	1 M KOH	(-0.9–0.1) V	222 F g^{-1} at 0.5 A g^{-1}	This work	VNNWs@rGO-2

4. Conclusion

In summary, a novel electrode material of VNNWs@rGO-2 with a special lamellar structural design was developed, in which nanocarved VN nanowires were encapsulated N-doped rGO sheets, and the 2D nanosheets were further interconnected to form a foam architecture. This structure design is beneficial for electronic transmission and ions diffusion. In VNNWs@rGO-2 electrode, the nanocarved structure of VN with numerous vacancy and active sites can absorb/desorb ions efficiently, which accounts for the excellent pseudocapacitance. Combined of the hierarchical layered structure, synergistic effects of N-doped rGO and VN, and rGO content modulation, VNNWs@rGO-2 electrode exhibited good electrochemical properties: high capacitances of 222 and 65 F g^{-1} were obtained at current densities of

0.5 and 10 A g^{-1}, respectively. The underlying electrochemical mechanism includes both EDLC and pseudocapacitance. As a result, preparing multi-dimensional VNNWs@rGO-2 with 1D nanovarved VN nanowires, 2D laminar rGO sheets, and 3D interconnected form structure provides a train of thought for synthesizing high- performance hybrid electrode materials for supercapacitors.

Declarations

Funding Sources

This work is founded by National Natural Science Foundation of China (No.52002233) and Shaanxi University of Science & Technology (2018BJ-59).

Conflicts of Interest

The authors declare no competing financial interest.

References

1. Q. Li, Y. Chen, J. Zhang et al., Nano Energy **51**, 128 (2018)
2. P. Jh Huo, X.F. Zheng, S.W. Wang, Guo, Appl Surf Sci **442**, 575 (2018)
3. J. Huo, Y. Xue, X. Zhang, S. Guo, Electrochim. Acta **292**, 639 (2018)
4. T. Wang, J. Liu, L. Kong, H. Yang, F. Wang, C. Li, Ceram. Int. **46**, 25392 (2020)
5. X. Jiang, W. Lu, X. Yu, S. Song, Y. Xing, Nanoscale Advances, (2020)
6. R. Adalati, A. Kumar, Y. Kumar, R. Chandra, Energy Technol-Ger n/a, 2000466 (2020)
7. Y. Tan, Y. Liu, Z. Tang et al., Sci. Rep. **8**, 2915 (2018)
8. C. Xie, S. Yang, X. Xu, J.-W. Shi, C. Niu, J. Nanopart. Res. **22**, 25 (2020)
9. H. Pang, S. Ee, Y. Dong, X. Dong, P. Chen, Chemelectrochem 1, (2014)
10. S. Dong, X. Chen, L. Gu et al., Mater. Res. Bull. **46**, 835 (2011)
11. M. Chen, H. Fan, Y. Zhang, X. Liang, Q. Chen, X. Xia, Small n/a, 2003434 (2020)
12. Y. Liu, L. Lingyang, L. Kang, F. Ran, J. Power Sources **450**, 227687 (2020)
13. H.-M. Lee, G.H. Jeong, S.-W. Kim, C.-K. Kim, Appl Surf Sci **400**, 194 (2017)
14. J. Balamurugan, G. Karthikeyan, T.D. Thanh, N.H. Kim, J.H. Lee, J. Power Sources **308**, 149 (2016)
15. Y. Wu, F. Ran, J. Power Sources **344**, 1 (2017)
16. Y. Wu, Y. Yang, X. Zhao et al., Nano-Micro Lett **10**, 63 (2018)
17. Y. Liu, L. Liu, Y. Tan et al., Electrochim. Acta **262**, 66 (2018)
18. X. Lu, M. Yu, T. Zhai et al., Nano Lett. **13**, 2628 (2013)
19. Y. Liu, J. Chang, L. Liu, L. Kang, F. Ran, New J Chem **44**, 6791 (2020)
20. Y. Liu, Q. Wu, L. Liu, P. Manasa, L. Kang, F. Ran, J Mater Chem A **8**, 8218 (2020)

21. A. Djire, P. Pande, A. Deb et al., Nano Energy **60**, 72 (2019)
22. J. Guo, Q. Zhang, J. Sun et al., J. Power Sources **382**, 122 (2018)
23. H. Liu, H. Zhang, H. Xu, T. Lou, Z. Sui, Y. Zhang, J Electrochem Soc **165**, A97 (2018)
24. X. Yuan, R. Wang, W. Huang et al., Chem. Eng. J. **378**, 122203 (2019)
25. B. Gao, X. Li, X. Guo et al., Advanced Materials Interfaces **2**, 1500211 (2015)
26. T. He, Z. Wang, X. Li et al., J. Alloy. Compd. **781**, 1054 (2019)
27. F. Ran, Y. Wu, M. Jiang et al., Dalton T **47**, 4128 (2018)
28. Y. Wang, M. Jiang, Y. Yang, F. Ran, Electrochim. Acta **222**, 1914 (2016)
29. G. Wang, S. Hou, C. Yan, X. Zhang, W. Dong, J. Mater. Sci.: Mater. Electron. **29**, 13118 (2018)
30. Y. Liu, L. Liu, L. Kong, L. Kang, F. Ran, Electrochim. Acta **211**, 469 (2016)
31. Y. Liu, L. Liu, Y. Tan, L. Kong, L. Kang, F. Ran, J. Phys. Chem. C **122**, 143 (2018)
32. A.M. Glushenkov, D. Hulicova-Jurcakova, D. Llewellyn, G.Q. Lu, Y. Chen, Chem. Mater. **22**, 914 (2010)
33. X. Chen, X. Chen, X. Xu et al., Nanoscale **6**, 13740 (2014)
34. H.-L. Guo, P. Su, X. Kang, S.-K. Ning, J Mater Chem A **1**, 2248 (2013)

Figures

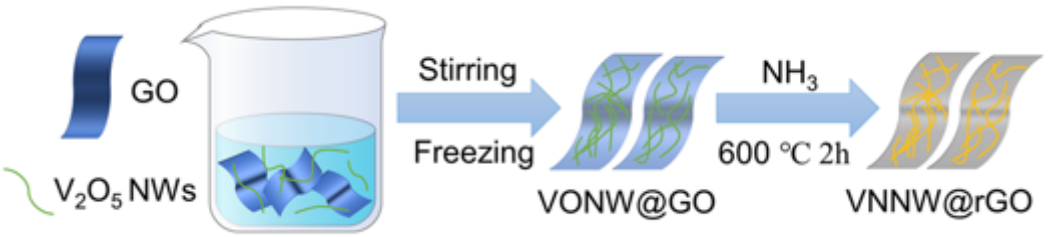

Figure 1

Schematic illustration of the synthesis procedure of VNNWs@rGO hierarchical structure.

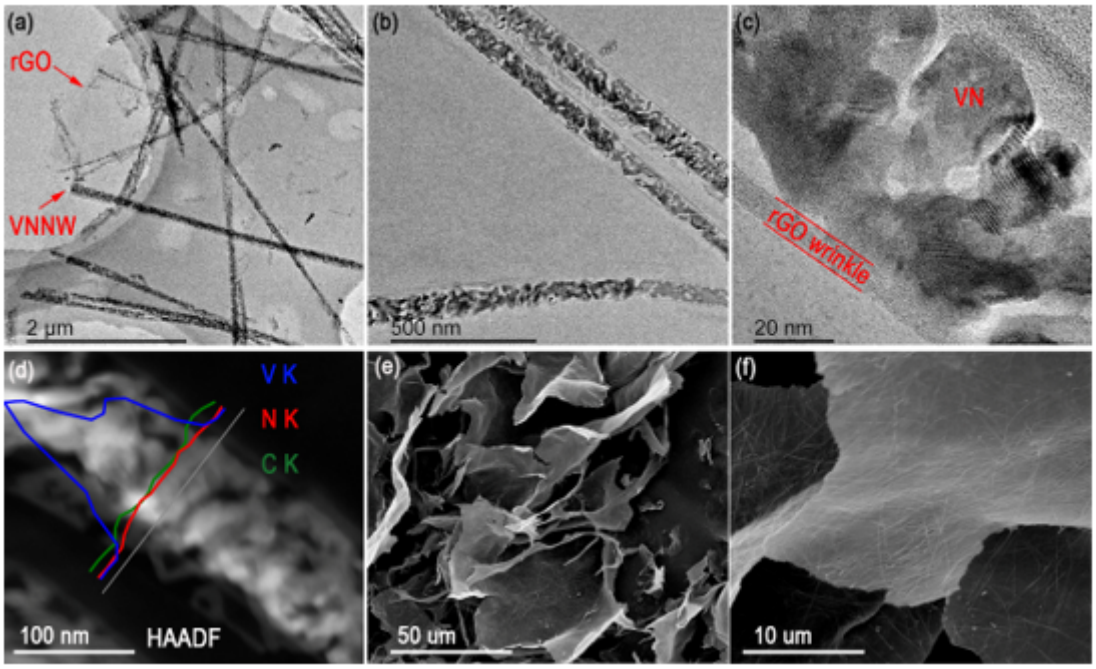

Figure 2

(a-c) TEM and (d) HAADF-STEM image with corresponding line profiles of V, N, and C elements in VNNWs@rGO-2; (e-f) SEM images of VNNWs@rGO-2.

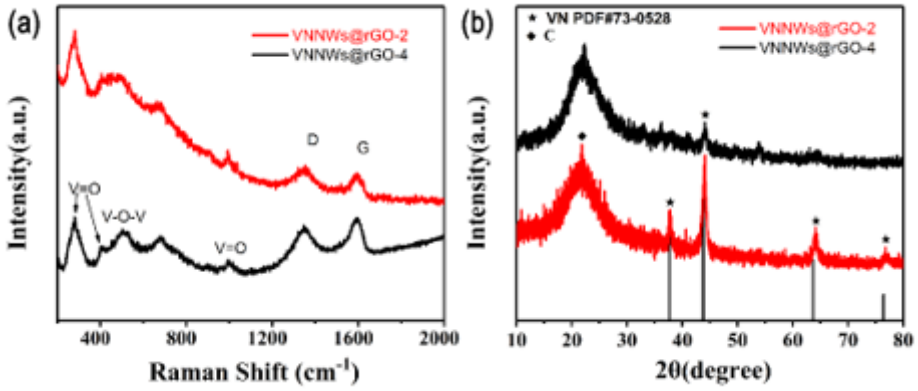

Figure 3

(a) Raman spectra and (b) XRD patterns of VNNWs@rGO-2 and VNNWs@rGO-4, where the diffraction peaks of carbon are marked by •, the diffraction peaks originated from VN are marked by □, and the information of PDF No.73–0528 is shown by black vertical lines at the bottom.

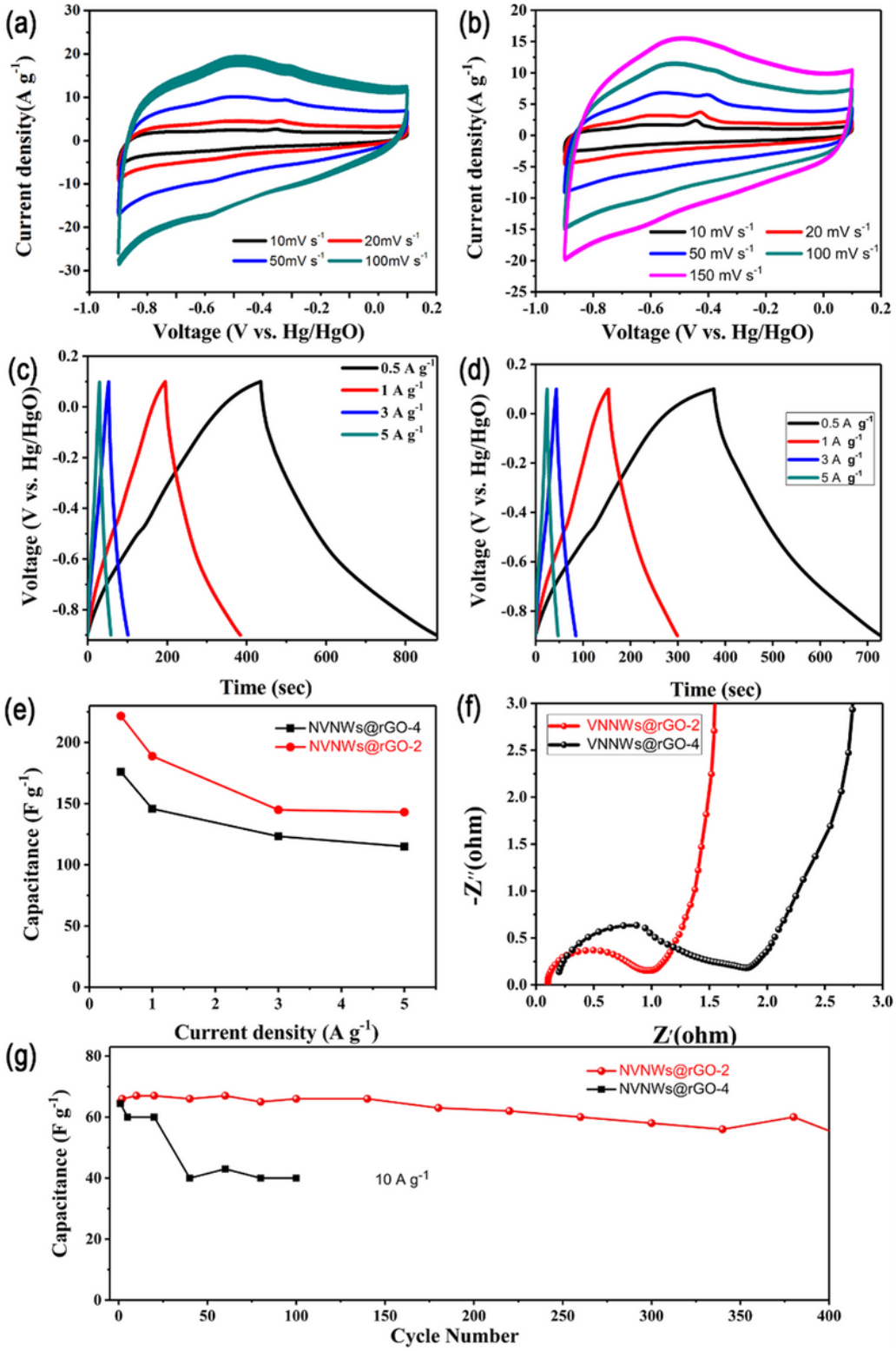

Figure 4

Electrochemical curves of VNNWs@rGO electrodes: CV curves at various scan rates (10, 20, 50, 100, 150 mV s-1) for (a) VNNWs@rGO-2 and (b) VNNWs@rGO-4; GCD curves at different current densities (0.5, 1, 3, 5 A g-1) for (c) VNNWs@rGO-2 and (d) VNNWs@rGO 4; (e) the relationship between mass specific capacitances and current densities for VNNWs@rGO-2 (red color) and VNNWs@rGO-4 (black color); (f)

EIS curves for VNNWs@rGO-2 (red color) and VNNWs@rGO-4 (black color); (g) the cycling performance at a current density of 10 A g-1.